

# Large-Scale Molecular Dynamics Simulations of Metal Sorption onto the Basal Surfaces of Clay Minerals

Sandia National Laboratories

**U.S. Nuclear Regulatory Commission  
Office of Nuclear Regulatory Research  
Washington, DC 20555-0001**



## AVAILABILITY OF REFERENCE MATERIALS IN NRC PUBLICATIONS

### NRC Reference Material

As of November 1999, you may electronically access NUREG-series publications and other NRC records at NRC's Public Electronic Reading Room at [www.nrc.gov/NRC/ADAMS/index.html](http://www.nrc.gov/NRC/ADAMS/index.html).

Publicly released records include, to name a few, NUREG-series publications; *Federal Register* notices; applicant, licensee, and vendor documents and correspondence; NRC correspondence and internal memoranda; bulletins and information notices; inspection and investigative reports; licensee event reports; and Commission papers and their attachments.

NRC publications in the NUREG series, NRC regulations, and *Title 10, Energy*, in the Code of *Federal Regulations* may also be purchased from one of these two sources.

1. The Superintendent of Documents  
U.S. Government Printing Office  
Mail Stop SSOP  
Washington, DC 20402-0001  
Internet: [bookstore.gpo.gov](http://bookstore.gpo.gov)  
Telephone: 202-512-1800  
Fax: 202-512-2250
2. The National Technical Information Service  
Springfield, VA 22161-0002  
[www.ntis.gov](http://www.ntis.gov)  
1-800-553-6847 or, locally, 703-605-6000

A single copy of each NRC draft report for comment is available free, to the extent of supply, upon written request as follows:

Address: Office of the Chief Information Officer,  
Reproduction and Distribution  
Services Section  
U.S. Nuclear Regulatory Commission  
Washington, DC 20555-0001  
E-mail: [DISTRIBUTION@nrc.gov](mailto:DISTRIBUTION@nrc.gov)  
Facsimile: 301-415-2289

Some publications in the NUREG series that are posted at NRC's Web site address [www.nrc.gov/NRC/NUREGS/indexnum.html](http://www.nrc.gov/NRC/NUREGS/indexnum.html) are updated periodically and may differ from the last printed version. Although references to material found on a Web site bear the date the material was accessed, the material available on the date cited may subsequently be removed from the site.

### Non-NRC Reference Material

Documents available from public and special technical libraries include all open literature items, such as books, journal articles, and transactions, *Federal Register* notices, Federal and State legislation, and congressional reports. Such documents as theses, dissertations, foreign reports and translations, and non-NRC conference proceedings may be purchased from their sponsoring organization.

Copies of industry codes and standards used in a substantive manner in the NRC regulatory process are maintained at—

The NRC Technical Library  
Two White Flint North  
11545 Rockville Pike  
Rockville, MD 20852-2738

These standards are available in the library for reference use by the public. Codes and standards are usually copyrighted and may be purchased from the originating organization or, if they are American National Standards, from—

American National Standards Institute  
11 West 42<sup>nd</sup> Street  
New York, NY 10036-8002  
[www.ansi.org](http://www.ansi.org)  
212-642-4900

Legally binding regulatory requirements are stated only in laws; NRC regulations; licenses, including technical specifications; or orders, not in NUREG-series publications. The views expressed in contractor-prepared publications in this series are not necessarily those of the NRC.

The NUREG series comprises (1) technical and administrative reports and books prepared by the staff (NUREG-XXXX) or agency contractors (NUREG/CR-XXXX), (2) proceedings of conferences (NUREG/CP-XXXX), (3) reports resulting from international agreements (NUREG/IA-XXXX), (4) brochures (NUREG/BR-XXXX), and (5) compilations of legal decisions and orders of the Commission and Atomic and Safety Licensing Boards and of Directors' decisions under Section 2.206 of NRC's regulations (NUREG-0750).

**DISCLAIMER:** This report was prepared as an account of work sponsored by an agency of the U.S. Government. Neither the U.S. Government nor any agency thereof, nor any employee, makes any warranty, expressed or implied, or assumes any legal liability or responsibility for any third party's use, or the results of such use, of any information, apparatus, product, or process disclosed in this publication, or represents that its use by such third party would not infringe privately owned rights.

# **Large-Scale Molecular Dynamics Simulations of Metal Sorption onto the Basal Surfaces of Clay Minerals**

---

Manuscript Completed: October 2001  
Date Published: February 2002

Prepared by  
D. M. Teter, R. T. Cygan

Sandia National Laboratories  
Albuquerque, NM 87185-0750

E. O'Donnell, NRC Project Manager

**Prepared for**  
**Division of Systems Analysis and**  
**Regulatory Effectiveness**  
**Office of Nuclear Regulatory Research**  
**U.S. Nuclear Regulatory Commission**  
**Washington, DC 20555-0001**  
**NRC Job Code W6811**



## Abstract

Large-scale molecular dynamics computer simulations have been completed to evaluate the sorption of  $\text{Cs}^+$ ,  $\text{Sr}^{2+}$ , and other related ions onto the (001) basal planes of kaolinite and montmorillonite. Simulations were undertaken as a function of metal ion concentration to evaluate sorption mechanisms and to determine distribution coefficients ( $K_d$ 's). The simulations show that  $\text{Cs}^+$  ions bind to both kaolinite and montmorillonite, while  $\text{Sr}^{2+}$  ions tend to remain in solution. At high ionic strengths (greater than 0.5 M), the fundamental mechanism for  $\text{Cs}^+$  sorption to the aluminol plane of kaolinite is through the formation of  $\text{CsCl}$  complexes where the  $\text{Cl}^-$  ion is loosely bound to the outer hydroxyl groups. At lower concentrations (0.1 M and 0.01 M), the  $\text{Cs}^+$  ions do not sorb to the aluminol plane, but prefer to bind adjacent to the center of the six-membered ring silica tetrahedral sheet as an inner-sphere complex. We have determined a  $K_d$  of  $10 \pm 4$  ml/g for kaolinite to sorb  $\text{Cs}^+$  ions from a 0.01M  $\text{CsCl}$  solution, and a  $K_d$  of 0 for kaolinite to sorb  $\text{Sr}^{2+}$  ions from a 0.01M  $\text{SrCl}_2$  solution. For the case of montmorillonite, we have determined a  $K_d$  of  $293 \pm 30$  ml/g to sorb  $\text{Cs}^+$  ions from a 0.1M  $\text{CsCl}$  solution, and a  $K_d$  of  $11 \pm 4$  ml/g to sorb  $\text{Sr}^{2+}$  ions from a 0.1M  $\text{SrCl}_2$  solution. The montmorillonite sorbs the cations more effectively than kaolinite because it has negatively-charged sorption sites that are created by isomorphic substitutions on both tetrahedral and octahedral sites. Calculations show that the  $\text{Sr}^{2+}$  ion is solvated more strongly than  $\text{Cs}^+$  and is not sorbed by the kaolinite or montmorillonite surfaces. Directions for further work are outlined and prioritized.

## Contents

Abstract .....	iii
Foreward .....	vii
Acknowledgments .....	viii
1. INTRODUCTION .....	1-1
2. MATERIAL AND FINITE ELEMENT ANALYSIS MODELS .....	2-1
2.1 Kaolinite Structure .....	2-1
2.2 Montmorillonite Structure .....	2-1
3. MOLECULAR MODELING METHODS .....	3-1
3.1 Validation of Interatomic Potentials .....	3-2
4. MOLECULAR MODELING RESULTS .....	4-1
4.1 Modeling the Kaolinite Unit Cell .....	4-1
4.2 The Solvation of Cs <sup>+</sup> in Water .....	4-1
4.3 Modeling of the Cs <sup>+</sup> Cl <sup>-</sup> Complex .....	4-2
4.4 Modeling of Cesium and Strontium Sorption onto the Kaolinite (001) Surface .....	4-3
4.4.1 Preliminary Simulations .....	4-3
4.4.2 Production Simulations .....	4-6
5. CALCULATION OF DISTRIBUTION COEFFICIENTS .....	5-1
5.1 Kaolinite .....	5-1
5.2 Montmorillonite .....	5-1
5.3 Energetics and K <sub>d</sub> Values .....	5-1
6. CONCLUSIONS .....	6-1
7. SUGGESTIONS FOR FURTHER WORK .....	7-1
8. REFERENCES .....	8-1

## Figures

Figure 1. A graphical representation of the <i>CI</i> unit cell of kaolinite. The top sheet is composed of $\text{AlO}_6$ octahedra (O) and the bottom sheet is composed of $\text{SiO}_4$ tetrahedra (T).....	2-1
Figure 2. A graphical representation of the unit cell of montmorillonite without interlayer cations and waters.....	2-2
Figure 3. A graphical representation of a $\text{Cs}^+$ ion hydrated by six waters in an octahedral geometry.....	4-2
Figure 4. Representative configuration for the preliminary analysis of the equilibrated $\text{Cs}^+$ sorption onto the (001) basal surfaces of kaolinite.....	4-4
Figure 5. Density profile of the equilibrated 1 M CsCl solution interacting with the two basal surfaces of kaolinite based on the accumulation of 100 psec of trajectory analysis from the preliminary molecular dynamics simulation.....	4-4
Figure 6. Density maps of the equilibrated 1 M CsCl solution interacting with the aluminol basal surface of kaolinite, based on the accumulation of 100 psec of trajectory analysis from the preliminary molecular dynamics simulation.....	4-5
Figure 7. Density maps of the equilibrated 1 M CsCl solution interacting with the siloxane basal surface of kaolinite based on the accumulation of 100 psec of trajectory analysis from the preliminary molecular dynamics simulation.....	4-6
Figure 8. A graphical representation of a 0.5 M CsCl solution in steady-state equilibrium with a (001) kaolinite surface.....	4-7
Figure 9. A graphical representation of a 0.1 M CsCl solution in steady-state equilibrium with a (001) kaolinite surface.....	4-7
Figure 10. A graphical representation of a 0.01 M CsCl solution in steady-state equilibrium with a (001) kaolinite surface.....	4-8
Figure 11. Details of the 0.01 M CsCl solution in steady-state equilibrium with a (001) kaolinite surface.....	4-8
Figure 12. A graphical representation of a 0.1 M $\text{Cs}^+$ solution in steady-state equilibrium with a (001) montmorillonite surface.....	4-9
Figure 13. A graphical representation of a 0.1 M $\text{Sr}^{2+}$ solution in steady-state equilibrium with a (001) montmorillonite surface.....	4-9
Figure 14. A graphical representation of 8 $\text{Cs}^+$ and 8 $\text{Sr}^{2+}$ ions in steady-state equilibrium with a (001) montmorillonite surface.....	4-9

## Tables

Table 1. Forcefield parameters used for the Coulombic and Lennard-Jones terms of the nonbonded potential energy expression represented by Equation (1). .....	3-1
Table 2. A comparison of the kaolinite unit cell parameters as determined by experiment, DFT-GGA calculations, and the forcefield parameters used in this study. ....	4-1
Table 3. Equilibrium $\text{Cs}^+$ - $\text{O}_{\text{water}}$ distances as the water coordination number increases calculated using density functional theory and the forcefield described in Table 1.....	4-2
Table 4. Calculation of the cohesive energy of the $\text{Cs}^+\text{Cl}^-$ complex as a function of ionic separation using DFT and the forcefield parameters described in Table 1. ....	4-2
Table 5. Comparison of energy for various ions based on water solvation or clay surface sorption environment....	5-2

## Foreword

This contractor technical report was prepared by Sandia National Laboratories under their Interagency Work Order (JCN W6811) with the U.S. Nuclear Regulatory Commission.

This report summarizes the results of a task to apply molecular dynamics computer simulations for the sorption of monovalent and divalent metallic cations onto clay minerals. In particular, the report focuses on the sorption of  $\text{Cs}^+$  and  $\text{Sr}^{2+}$ . The results of these simulations give insights into the basic mechanisms controlling metal sorption onto common soil components such as clay minerals. The information on mechanisms controlling sorption reported here are being applied by Sandia to enhance the prediction of radionuclide transport through soil.

This report is not a substitute for NRC regulations, and compliance is not required. The approaches and/or methods described in this NUREG/CR report are provided for information only. Publication of this report does not necessarily constitute NRC approval or agreement with the information contained herein. Use of product or trade names is for identification purposes only and does not constitute endorsement by the NRC or Sandia National Laboratories.



Cheryl A. Trotter, Chief  
Radiation Protection, Environmental Risk, and Waste Management Branch  
Division of Systems Analysis and Regulatory Effectiveness  
Office of Nuclear Regulatory Research

## Acknowledgments

Special thanks are extended to Andrey Kalinichev for his assistance in performing the atom density maps in the analysis of the preliminary kaolinite simulations. The reviews provided by Louise Criscenti and Henry Westrich of an early draft of the manuscript are gratefully acknowledged. This work was supported by the U.S. Nuclear Regulatory Commission, Office of Nuclear Regulatory Research. We are very grateful for the advice and support provided by our NRC program manager, Dr. Edward O'Donnell, during the funding period. Sandia National Laboratories is a multiprogram laboratory operated by the Sandia Corporation, a Lockheed Martin Company, for the United States Department of Energy under Contract DE-AC04-94AL85000.

## 1. INTRODUCTION

Radioactive  $^{137}\text{Cs}$  and  $^{90}\text{Sr}$  have been dispersed globally by nuclear testing, the production of weapons grade uranium and plutonium, and more recently by the nuclear accident at Chernobyl. The fate of  $^{137}\text{Cs}$  and other radionuclides in the environment is controlled primarily by the ability of subsurface and colloidal minerals to naturally attenuate these contaminants through irreversible sorption and precipitation processes.  $^{137}\text{Cs}$  is also a concern because of the phenomena known as "cask weeping", whereupon initially sorbed  $^{137}\text{Cs}$  desorbs from nuclear fuel transport casks during shipping due to changes in environmental chemistry (Teter *et al.*, work in progress at SNL). Our ability to evaluate these processes is based on experimental methods such as surface charge titrations, sorption isotherm measurements, atomic force microscopy (AFM), nuclear magnetic resonance (NMR) and X-ray adsorption spectroscopies (EXAFS and XANES). However, despite the power of the available analytical methods, many of the details of the sorption process elude us because of the structural and chemical complexities of geomedia such as clays. The application of atomistic methods allows us to construct and test detailed models of chemical and physical processes such as sorption. When combined with experiments, these methods can provide a fundamental understanding of sorption mechanisms that en-

ables us to design more efficient methods for waste treatment and improve the immobilization and sequestration of contaminants (Krumhansl *et al.*, 2001).

We are studying the sorption of  $\text{Cs}^+$  and  $\text{Sr}^{2+}$  on kaolinite surfaces because kaolinite provides a relatively simple substrate for studying surface sorption due to its lack of interlayer metal sites. The sorption of  $\text{Cs}^+$  on kaolinite has been experimentally verified by Kim *et al.* (1996a, 1996b, 1997, 1998), Komarneni (1978), Krumhansl *et al.* (2001), Michaelian (1998a, 1998b), Sayers and Hornberger (1999), Weiss *et al.* (1990), and Westrich *et al.* (1996). The sorption isotherms suggest a pH-dependent affinity of Cs for the Al octahedral edge sites, with possibly weak sorption on the Si tetrahedral edge sites at high-pH values. Binding of  $\text{Cs}^+$  to the basal Al octahedral sites appears to be independent of pH. These results are supported by titration experiments to determine the effect of pH on the surface charge of kaolinite and the subsequent surface complexation modeling (Brady *et al.* 1996, 1998). Nagy *et al.* (1995) obtained AFM images of individual kaolinite grains that provide evidence for significant edge surface area, possibly up to 50% of the surface area. These AFM images provide additional support for the strong influence of edge sites on Cs sorption.

## 2. MATERIAL AND FINITE ELEMENT ANALYSIS MODELS

### 2.1 Kaolinite Structure

Kaolinite ( $\text{Al}_2\text{Si}_2\text{O}_5(\text{OH})_4$ ) is one of the simplest layered clays. Kaolinite is a layered aluminosilicate with a 1:1 uncharged layered structure. Each layer consists of a sheet of  $\text{AlO}_6$  octahedra (O) building four-membered aluminate rings that are connected via common oxygen atoms to a sheet of  $\text{SiO}_4$  tetrahedra (T) forming six-membered silicate rings. Only two of the three possible aluminum sites are occupied in the octahedral layer. The kaolinite structure contains two types of hydroxyl groups, both of which are contained in the Al octahedral sheet. The interlayer hydroxyl groups are bound to the hexa-coordinated aluminum atoms and cover one of the two basal surfaces of each layer. These hydroxyl groups form hydrogen bonds with the adjacent Si tetrahedral sheet in the next TO layer repeated in the (001) direction. The inner hydroxyl groups are situated within the shared plane of the octahedral/tetrahedral sheets and are associated with the vacant octahedral Al sites.

To examine the specific molecular controls on Cs sorption, we used an atomistic model of a kaolinite surface derived from the unit cell shown in Figure 1. This model is based upon the unit cell parameters recently determined by Neder *et al.* (1999) in a single-crystal

structure refinement using synchrotron radiation, with the internal parameters determined by Bish (1989, 1993) from Rietveld refinement of the neutron powder data. These unit cell parameters agree well with the previous studies by Young and Hewatt (1988) and Adams (1983).

### 2.2 Montmorillonite Structure

Montmorillonite (approximately  $\text{Na}_3(\text{Si}_{31}\text{Al})(\text{Al}_{14}\text{Mg}_2)\text{O}_{80}(\text{OH})_{16}\cdot n\text{H}_2\text{O}$ ) where this formula represents four formula units and is comprised of an octahedral sheet, is sandwiched between two tetrahedral sheets and is classified as a 1:2 layer silicate mineral. In contrast to kaolinite, montmorillonite has a layered structure that possesses a net negative charge due to isomorphic substitutions of metal ions in either the tetrahedral, octahedral, or both sheets. Typically, aluminum substitutes for silicon atoms in the tetrahedral sheet and magnesium for aluminum in the octahedral sheet (see formula). The charge deficiency allows for the introduction of interlayer cations, often hydrated by water molecules, that balance out the negative layer charge. The relatively small charge imbalance of the layer structure and the strength of the hydrogen bonding associated with the interlayer waters, allow montmorillonite clays to swell, like other smectite clays. The

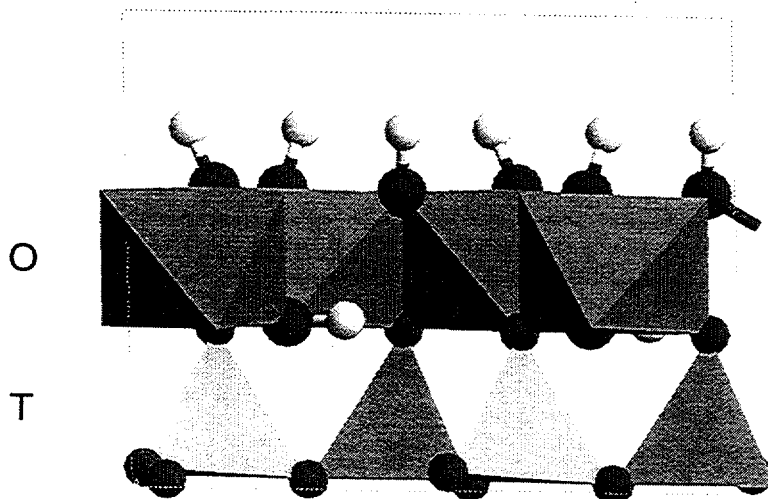
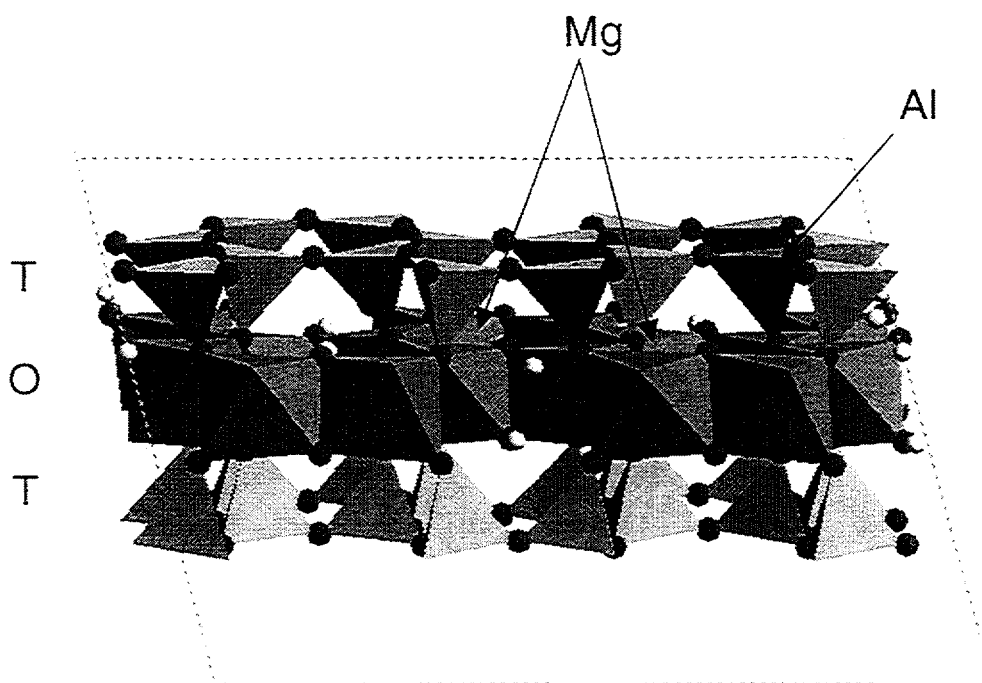


Figure 1. A graphical representation of the *1:1* unit cell of kaolinite. The top sheet is composed of  $\text{AlO}_6$  octahedra (O) and the bottom sheet is composed of  $\text{SiO}_4$  tetrahedra (T). The interlayer hydroxyls are visible above the O sheet and the inner hydroxyls are visible between the O and T sheets.

octahedral layer consists of a sheet of  $\text{AlO}_6$  that form four-membered aluminate rings. These rings are connected via common oxygen atoms to two sheets of  $\text{SiO}_4$  tetrahedra, forming six-membered silicate rings. Like kaolinite, only two of the three possible aluminum sites are occupied in montmorillonite; both clay minerals are often referred to as dioctahedral clays. The hydroxyl groups of montmorillonite are situated within both of the shared planes and are associated with the vacant octahedral aluminum sites. Refined structures for montmorillonite and other smectite clays are lacking in

literature, due to the sub-micron grain size of these materials, which prevents any quality single crystal refinement, and the extensive stacking disorder that occurs in the z-direction which precludes the long range ordering needed to enhance diffraction signals. Fortunately, there have been several conceptual models for montmorillonite which provide a sound basis for the crystal structure. The montmorillonite model presented in Figure 2 is based on the electron diffraction determination by Tzipursky and Drits (1984).



**Figure 2.** A graphical representation of the unit cell of montmorillonite without interlayer cations and waters. The top and bottom sheets are composed of  $\text{SiO}_4$  tetrahedra (T), while the middle sheet is composed of  $\text{AlO}_6$  octahedra (O). The darkened tetrahedra in the top right sheet represents an aluminum substitution, while the two light octahedra in the middle rear sheet represent magnesium substitutions (note arrows). These substitutions create negatively charged sites that are normally charged balanced by interlayer Na ions.

### 3. MOLECULAR MODELING METHODS

The computer simulation methods in this study determine the potential energy of the system using a set of analytical functions referred to as forcefields. This model calculates the energy and forces in the system based upon the atomic coordinates of the atoms. Energy contributions are derived from non-bonded interactions, such as the long-range Coulombic terms, as well as short-range repulsions and attractive Van der Waals interactions. Contributions to the potential energy also arise from bonded terms such as bond stretching and bond angle bending terms.

The non-bonded interactions are the critical energy contributions that will control how a molecule or ion will approach and interact with a mineral surface. The analytical expression (Equation (1)) for the non-bonded energy expression includes the Coulombic and Lennard-Jones potential terms. The potential energy  $U_{ij}$  for the interaction between ion  $i$  and ion  $j$  at an ionic separation of  $r_{ij}$  is given by:

$$U_{ij} = \frac{q_i q_j}{r_{ij}} + 4\epsilon_{ij} \left[ \left( \frac{\sigma_{ij}}{r_{ij}} \right)^{12} - \left( \frac{\sigma_{ij}}{r_{ij}} \right)^6 \right] \quad (1)$$

where  $q_i$  and  $q_j$  are the ionic charges. The Lennard-Jones parameters,  $\epsilon_{ij}$  and  $\sigma_{ij}$  represent the potential well depth (in kJ/mol) and the interatomic distance (in Å) at the energy minimum. The first term of Equation (1) represents the Coulombic energy and

can be either positive or negative, depending on the charges on the interacting ions and is the dominant non-bonded energy term. The next two terms represent the short-range repulsive energy term and the attractive Van der Waals term as a function of ionic separation. The forcefield parameters used in this study are given in Table 1 with the short-range parameters determined using the mixing rules given in Equations (2a) and (2b):

$$\epsilon_{ij} = \sqrt{\epsilon_i \epsilon_j} \quad \sigma_{ij} = \frac{\sigma_i + \sigma_j}{2} \quad (2a,b)$$

The bonded interactions within the water molecule and hydroxyl groups are treated as harmonic oscillators (Eq. 3):

$$U_{\text{int}}(x) = \left( \frac{k_e}{2} \right) (x - x_e)^2 \quad (3)$$

where  $x$  is an interatomic bond length or angle,  $x_e$  is its corresponding equilibrium value and  $k_e$  the force constant. For the flexible SPC water model (Telemen *et al.*, 1987) used in this study, the bond stretching force constant for the water hydroxyl groups is  $k_e^{OH} = 4637 \text{ kJ mol}^{-1} \text{ Å}^{-2}$  and the equilibrium bond length is  $x_e^{OH} = 1.0 \text{ Å}$ , while the bond angle force constant is  $383 \text{ kJ mol}^{-1} \text{ rad}^{-2}$ , and the equilibrium H-O-H bond angle is  $109.47^\circ$ .

**Table 1. Forcefield parameters used for the Coulombic and Lennard-Jones terms of the nonbonded potential energy expression represented by Equation (1).**

Ion	Charge	$\epsilon$ (kJ/mol)	$\sigma$ (Å)	Reference
Al <sub>oct</sub>	+1.575	$5.567 \times 10^{-6}$	4.271	Cygan <i>et al.</i> (2002)
Mg <sub>oct</sub>	+1.360	$0.902 \times 10^{-6}$	5.265	Cygan <i>et al.</i> (2002)
Si <sub>tet</sub>	+2.100	$7.706 \times 10^{-6}$	3.302	Cygan <i>et al.</i> (2002)
H <sub>hydroxyl</sub>	+0.425	0.0000	0.000	Cygan <i>et al.</i> (2002)
O <sub>hydroxyl</sub>	-0.950	0.6502	3.166	Cygan <i>et al.</i> (2002)
O <sub>bond</sub>	-1.050	0.6502	3.166	Cygan <i>et al.</i> (2002)
Cs <sup>+</sup>	+1.000	0.0800	4.650	This study
Na <sup>+</sup>	+1.000	0.1000	2.750	This study
Sr <sup>2+</sup>	+2.000	0.0900	3.700	This study
Cl <sup>-</sup>	-1.000	0.1600	4.650	This study
H <sub>water</sub>	+0.410	0.0000	0.000	Telemen <i>et al.</i> (1987)
O <sub>water</sub>	-0.820	0.6502	3.166	Telemen <i>et al.</i> (1987)

### **3.1 Validation of Interatomic Potentials**

A critical stage of any model is validating it against the best available results before extending to predict new phenomena. In order to validate the forcefield

parameters to be used in this study, we compared their ability to reproduce experimental findings, as well as results obtained using quantum mechanical calculations. The following sections describe the ability of these forcefields to reproduce the kaolinite unit cell, the structure of  $\text{Cs}^+$  water clusters and the structure and energetics of the  $\text{CsCl}$  complex.

## 4. MOLECULAR MODELING RESULTS

### 4.1 Modeling the Kaolinite Unit Cell

The equilibrium unit cell parameters of kaolinite were calculated using an energy minimization scheme implementing the forcefield parameters. These results (Table 2) compare favorably with the recent experimental study by Neder *et al.* (1999) using synchrotron radiation. Furthermore, we used density functional theory (DFT) (Hohenberg and Kohn, 1964; Kohn and Sham, 1965) within the PW91 (Perdew and Wang, 1992) generalized gradient approximation (GGA) for electronic exchange and correlation to calculate the zero-pressure kaolinite unit cell. These calculations used ultrasoft pseudopotentials (Vanderbilt, 1990) with a plane-wave basis set (Pickett, 1989). A kinetic energy cut-off of 500 eV and a [222] Monkhorst-Pack Brillouin zone (Monkhorst and Pack, 1976) was used for the calculation. The kaolinite unit cell parameters determined by the forcefield calculations compare favorably with those determined using DFT. These results suggest that the forcefield parameters used in this study are capable of modeling the kaolinite surface with a reasonable degree of accuracy.

### 4.2 The Solvation of Cs<sup>+</sup> in Water

In order to validate the ability of the Cs<sup>+</sup> forcefield (Smith and Dang, 1994b) used in this study, we undertook a series of simulations to determine the ability of this forcefield to model Cs<sup>+</sup> solvation in an aqueous solution.

The solvation of a Cs<sup>+</sup> ion in water was investigated using molecular dynamics simulations. The computer

simulation consisted of a 18 Å x 18 Å x 18 Å box containing 200 water molecules and a Cs<sup>+</sup> ion using the forcefield parameters given in Table 1. An NVT (constant number of ions, constant volume, and constant temperature) molecular dynamics simulation was performed at a temperature of 300K using a timestep of 0.0005 psec to capture the high frequency hydroxyl vibrations. At equilibrium (5 psec), the radial distribution function indicates a coordination of approximately eight water molecules in the first coordination sphere at a mean distance of approximately 3.1 Å from the Cs<sup>+</sup> ion. X-ray and neutron diffraction studies (Ohtaki and Radnai, 1993) suggest a coordination of either six or eight, with Cs-O distances of 3.12 Å or 2.95 Å based upon two separate studies. The agreement of the aqueous simulation results with the experimental data provides some validation in the use of the selected forcefield parameters.

We then tested the ability of the Cs<sup>+</sup> potential to model discrete water clusters with the number of water molecules in the inner solvation sphere ranging from one to six. Figure 3 shows the Cs<sup>+</sup> ion being solvated by six water molecules in octahedral coordination. These results were compared to those derived from quantum mechanical calculations and were performed using the molecular DMol<sup>3</sup> code (Delley, 2000). These calculations were performed within the GGA-PW91 exchange and correlation functional, using a double numerical plus polarization (*dnp*) basis set, with a fine numerical integration grid and an octahedral expansion of the multipole densities. The Cs<sup>+</sup>-O<sub>water</sub> distances shown in Table 3 are fully converged with respect to the basis set and the numerical integration grid.

**Table 2. A comparison of the kaolinite unit cell parameters as determined by experiment, DFT-GGA calculations, and the forcefield parameters used in this study.**

	Experiment (Neder <i>et al.</i> , 1999)	DFT-GGA (this study)	Forcefield (this study)
<b>a</b> (Å)	5.154	5.199	5.169
<b>b</b> (Å)	8.942	9.018	8.923
<b>c</b> (Å)	7.401	7.455	7.253
<b>α</b>	91.69°	91.73°	91.68°
<b>β</b>	104.61°	104.64°	104.62°
<b>γ</b>	89.82°	89.85°	90.46°
<b>V</b> (Å <sup>3</sup> )	329.91	338.01	323.31

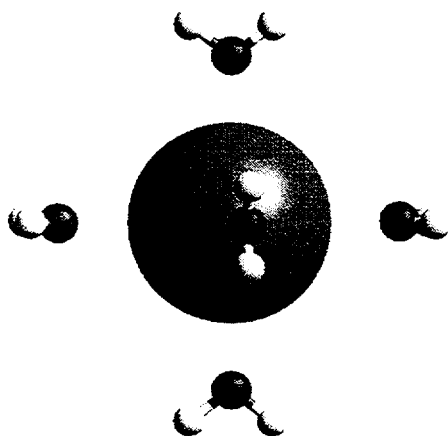


Figure 3. A graphical representation of a  $\text{Cs}^+$  ion hydrated by six waters in an octahedral geometry. The sixth water molecule is hidden by the sphere representing the cesium ion.

The  $\text{Cs}^+\text{-O}_{\text{water}}$  distances calculated using the forcefield compare favorably with those calculated using density functional theory. The  $\text{Cs}^+\text{-O}_{\text{water}}$  distances increase with the water coordination number, because, as more water molecules are packed around a  $\text{Cs}^+$  ion, they will strive to have a larger  $\text{O}_{\text{water}}\text{-O}_{\text{water}}$  separation. This result further validates the  $\text{Cs}^+$  potential as being suitable for modeling  $\text{Cs}^+$  in an aqueous solution.

### 4.3 Modeling of the $\text{Cs}^+\text{Cl}^-$ Complex

As a final validation of the  $\text{Cs}^+$  and  $\text{Cl}^-$  forcefield parameters, we calculated the equilibrium bond length for a  $\text{Cs}^+\text{Cl}^-$  complex and the cohesive energy as a function of  $\text{Cs}^+\text{-Cl}^-$  separation. These results were compared to those derived from quantum mechanical calculations using the Molecular Dynamics code.

Table 3. Equilibrium  $\text{Cs}^+\text{-O}_{\text{water}}$  distances as the water coordination number increases calculated using density functional theory and the forcefield described in Table 1.

Cluster	DFT-GGA $R(\text{Cs-O})$ (Å)	Forcefield $R(\text{Cs-O})$ (Å)
$\text{Cs}^+ + 1 \text{H}_2\text{O}$	3.014	2.982
$\text{Cs}^+ + 2 \text{H}_2\text{O}$	3.062	2.990
$\text{Cs}^+ + 3 \text{H}_2\text{O}$	3.073	3.003
$\text{Cs}^+ + 4 \text{H}_2\text{O}$	3.101	3.019
$\text{Cs}^+ + 6 \text{H}_2\text{O}$	3.180	3.059

Table 4. Calculation of the cohesive energy of the  $\text{Cs}^+\text{Cl}^-$  complex as a function of ionic separation using DFT and the forcefield parameters described in Table 1.

$R(\text{Cs}^+\text{-Cl}^-)$ (Å)	DFT-GGA (kcal/mol)	Forcefield (kcal/mol)
2.5	-95.201	15.3228
3.0	-112.160	-95.699
3.5	-102.921	-93.084
4.0	-90.436	-82.869
4.5	-79.571	-73.879
5.0	-71.018	-66.528

These calculations were performed within the GGA-PW91 exchange and correlation functional using a *dnp*-basis set, with a fine numerical integration grid and an octahedral expansion of the multipole densities. The  $R(\text{Cs}^+-\text{Cl}^-)$  distances shown in Table 4 are fully converged with respect to the basis set and the numerical integration grid.

The equilibrium separation determined using the forcefield (3.153 Å), is slightly larger than that obtained from DFT (2.933 Å). The energetics derived from the forcefield show smaller binding energies and a far stronger repulsive nature at close distances. However, in the region of interest (3.0 Å and greater), the forcefield reproduces the DFT results reasonably well and is applicable to the modeling of  $\text{Cs}^+\text{Cl}^-$  complexes in an aqueous solution.

## 4.4 Modeling of Cesium and Strontium Sorption onto the Kaolinite (001) Surface

### 4.4.1 Preliminary Simulations

#### 4.4.1.1 Kaolinite

Large-scale molecular dynamics simulations to simulate the sorption of  $\text{Cs}^+$  and  $\text{Sr}^{2+}$  ions on the (001) surfaces of kaolinite and montmorillonite, were performed using the forcefield parameters presented in Table 1. Preliminary simulations were performed on a four-processor SGI workstation using the OFF molecular dynamics code (Molecular Simulations Inc., 1999). Production calculations were completed using an MPI-parallelized version of the GULP 1.3 code (Gale, 1997) on SGI Origin2000 supercomputers at Sandia National Laboratories. The GULP 1.3 code scales near-linearly with the number of processors and is able to take advantage of the high floating-point performance processors available on the SGI Origin2000. The different codes and platforms used in these simulations represent an effective use of computational facilities. The development of the clay forcefield and preliminary simulations were run on a Unix workstation with one to four processors. The preliminary simulations, including the one noted below, required anywhere from approximately three to four days to two weeks to complete, while the production simulations on the massively parallel supercomputers were typically completed in a day. Unfor-

tunately, most of the computational cost of the latter simulations was due to queuing and preprocessing requirements.

Figure 4 provides the simulation cell used in the preliminary analysis of the sorption of a 1 M CsCl solution onto two unique basal surfaces of kaolinite. This system was used as a basis for determining the suitability of the clay forcefield for the sorption simulations and for troubleshooting the approach prior to performing the production simulations. The periodic simulation cell was created as a 4 x 4 x 2 supercell of the kaolinite unit cell. The CsCl solution was first equilibrated, separate from the kaolinite, using molecular dynamics and an NVT ensemble for 100 psec. The solution and kaolinite substrate, comprised of approximately 2400 atoms, were then equilibrated together at 300 K for 100 psec and then for an additional equilibrated period of 100 psec.

The equilibrated trajectory from the preliminary CsCl simulations was analyzed by running a density and probability algorithm to extract the positions for each atom during the 100 psec period. The density profile normal to the kaolinite surfaces for the equilibrated part of the 1 M CsCl simulation with kaolinite, is presented in Figure 5. The density plot indicates the relatively diffuse and weak structure of the solution components relative to the sharp density peaks for the crystalline components. The only exception to this is the  $\text{Cl}^-$  peak that occurs at the aluminol surface and which represents the strongly sorbed inner-sphere complex. In general, the  $\text{Cl}^-$  sorbs to the positively-charged aluminol surface while the  $\text{Cs}^+$  sorbs to the negatively-charged siloxane surface. The density profile supports this statement; however, some  $\text{Cs}^+$  also sorbs with the  $\text{Cl}^-$  as an ion pair onto the aluminol surface, as indicated by less intense Cs peak at aluminol surface, and which is not unexpected for the fairly concentrated CsCl solution. Cesium also occurs at the siloxane surface as a small peak at 2 Å (inner-sphere complex) and as a more diffuse peak at 5 Å (outer-sphere complex). An additional peak for  $\text{Cl}^-$  occurs at 12 Å, indicating an adsorbed outer-sphere complex on the aluminol surface. Hydrogen and oxygen profiles are typically diffuse across the profile, except for the near interface region where surface-controlled hydrogen bonding occurs to provide some structure. Water molecule orientations occur with the water dipole directing the hydrogens to the siloxane surface and oxygens to the aluminol surface.

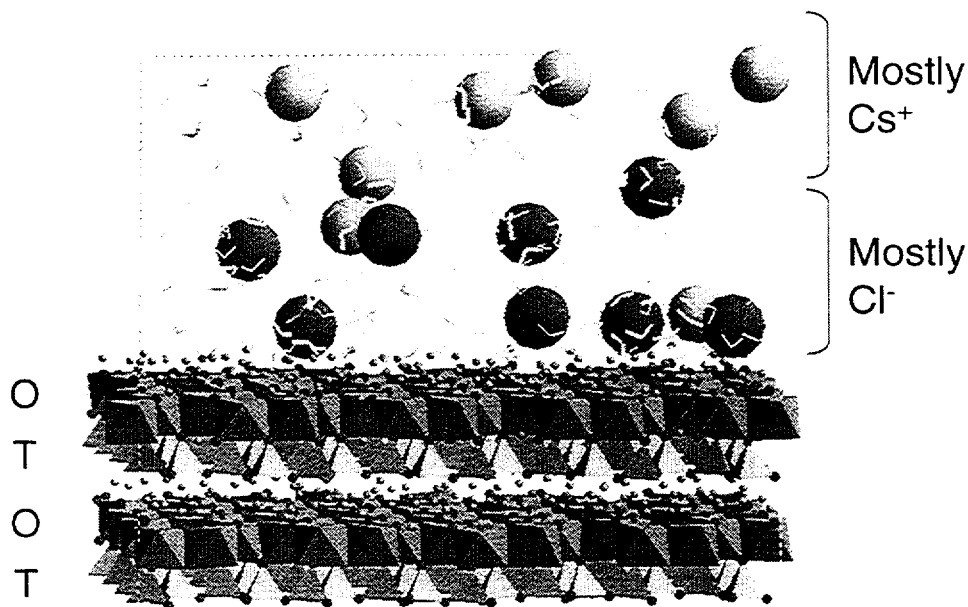


Figure 4. Representative configuration for the preliminary analysis of the equilibrated  $\text{Cs}^+$  sorption onto the (001) basal surfaces of kaolinite. The smaller  $\text{Cs}^+$  spheres sorb primarily to the tetrahedral siloxane surface, while the larger  $\text{Cl}^-$  spheres coordinate to the aluminol surface. Note that the simulation is periodic in three dimensions and that both basal surfaces of kaolinite are available to the  $\text{CsCl}$  solution. The very small spheres immediately above the kaolinite surface are the hydrogen atoms associated with the aluminol groups.

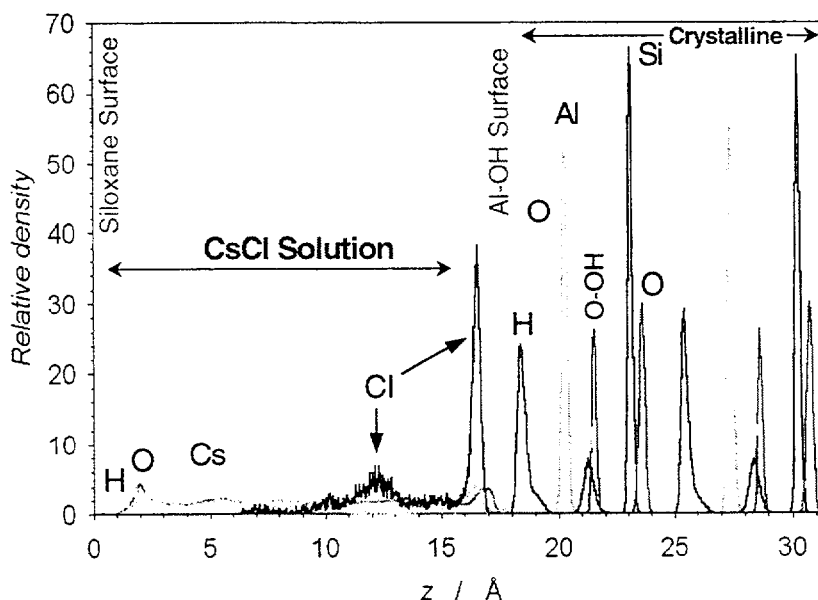


Figure 5. Density profile of the equilibrated 1 M  $\text{CsCl}$  solution interacting with the two basal surfaces of kaolinite based on the accumulation of 100 psec of trajectory analysis from the preliminary molecular dynamics simulation. The crystalline kaolinite is represented by the narrow and structured peaks on the right, and the solution species are denoted by the more diffuse peaks on the left. The strongly sorbing  $\text{Cl}^-$  is indicated by the distinct peak at the aluminol interface.

A more detailed density plot of the equilibrated kaolinite-CsCl solution is provided in Figures 6 and 7 where atomic density maps exhibit the contours for the occurrence of inner and outer-sphere complexes on the kaolinite surfaces. Figure 6 presents the results for the aluminol surface where the  $\text{Cl}^-$  sorption sites clearly occur as inner-sphere complexes above the aluminum vacancies. Cesium also exists as an inner-sphere complex on this surface, but only when coordinated to the sorbed  $\text{Cl}^-$ . Hydrogen atoms of the aluminol groups are displaced appropriately, based on their proximity to the  $\text{Cs}^+$  and  $\text{Cl}^-$ . The outer-sphere density map shows more diffuse contours for the  $\text{Cl}^-$  complexes indicating the greater mobility of the sorbed species in this region above the kaolinite aluminol surface. One of the inner-sphere  $\text{Cl}^-$  exhibits some transitory behavior into the outer-sphere region. Again,  $\text{Cs}^+$  only occurs when associated with the sorbed  $\text{Cl}^-$  species as an ion pair complex. Sorption site densities derived from the density maps are  $0.27 \text{ Cs}^+/\text{nm}^2$  and  $1.0 \text{ Cl}^-/\text{nm}^2$ .

The corresponding density maps for the siloxane surface of kaolinite are dominated by the sorption of  $\text{Cs}^+$ ; there is no occurrence of  $\text{Cl}^-$  sorption as either an inner or outer-sphere complex on this surface. Ce-

sium sorption is observed as both inner and outer-sphere complexes (Figure 7). As an inner-sphere complex,  $\text{Cs}^+$  primarily binds at the center of the hexagonal ring of the siloxane surface. Also, it is occasionally observed directly above the  $\text{SiO}_4^{4-}$  tetrahedra of the ring. The outer-sphere density map exhibits significantly diffuse contours for  $\text{Cs}^+$ , indicating a less strongly bound complex. As observed for  $\text{Cl}^-$  on the aluminol surface,  $\text{Cs}^+$  exhibits dynamic motion and goes through transitions between inner and outer-sphere complexes. The sorption site density is  $0.65 \text{ Cs}^+/\text{nm}^2$  on the siloxane surface of kaolinite.

Distribution coefficient can be derived from the equilibrated simulation by a comparison of sorbed  $\text{Cs}^+$  with the  $\text{Cs}^+$  still remaining in solution. Approximately 65 % of the  $\text{Cs}^+$  is sorbed as either an inner or outer-sphere complex. This corresponds to a  $K_d$  value of 0.0024, which if extrapolated to more applicable solution concentrations of 0.001 M CsCl, corresponds to a  $K_d$  of 24 ml/g. This value is in reasonable agreement with the experimental value of 12 ml/g (Brady *et al.*, 1998). More details on the method used to calculate  $K_d$  values are provided below.

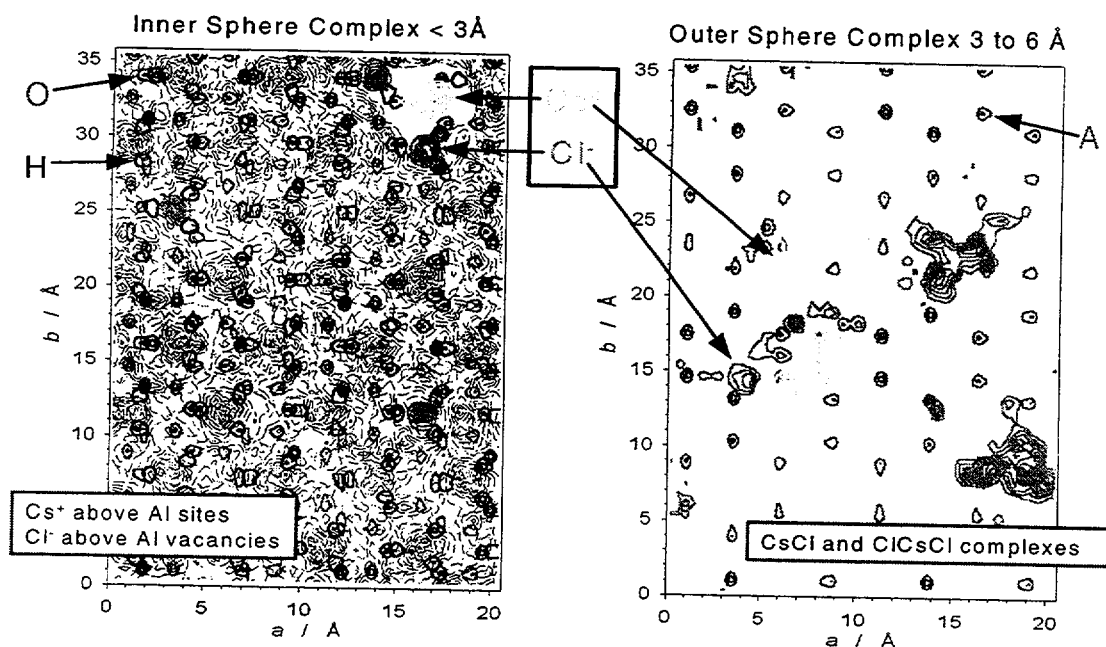
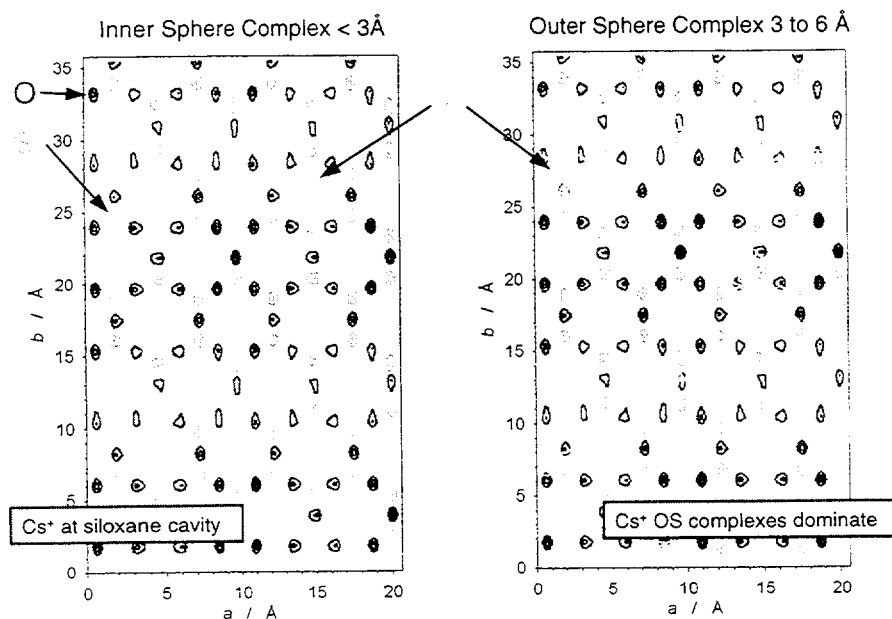


Figure 6. Density maps of the equilibrated 1 M CsCl solution interacting with the aluminol basal surface of kaolinite, based on the accumulation of 100 psec of trajectory analysis from the preliminary molecular dynamics simulation. The left figure indicates the inner-sphere region within 3 Å of the aluminol surface and the outer-sphere region between 3 Å to 6 Å is on the right. The hexagonal structure of the underlying aluminum and oxygen sublattices are provided in each density map.



**Figure 7.** Density maps of the equilibrated 1 M CsCl solution interacting with the siloxane basal surface of kaolinite based on the accumulation of 100 psec of trajectory analysis from the preliminary molecular dynamics simulation. The left figure indicates the inner-sphere region within 3 Å of the siloxane surface, and the outer-sphere (OS) region between 3 Å to 6 Å is on the right. The hexagonal structure of the underlying silicon and oxygen sublattice is provided in each density map.

## 4.4.2 Production Simulations

### 4.4.2.1 Kaolinite

A two-layer slab model of the kaolinite (001) surface was created using an 8 x 4 x 2 supercell of the kaolinite unit cell. The interlayer distance was increased by 32 Å and populated with 1670 H<sub>2</sub>O molecules. This system was then equilibrated using an NVT molecular dynamics scheme for 20 psec with a time-step of 0.001 psec. After reaching equilibrium, 15 Cs<sup>+</sup> and 15 Cl<sup>-</sup> ions (0.5 M CsCl) were inserted halfway along the interlayer distance and allowed to relax using an energy minimization scheme. A series of ten constant-NVT molecular dynamics runs were completed using a time-step of 0.001 psec and a simulation length of 500 psec. In all of these simulations, the dominant mechanism for Cs<sup>+</sup> sorption onto the aluminol surface was through the formation of Cs<sup>+</sup>Cl<sup>-</sup> complexes and their subsequent binding to the outer hydroxyl groups (Figure 8). A series of ten simulations of a ~0.1M CsCl solution interacting with the (001) kaolinite surface were undertaken by reducing the number of Cs<sup>+</sup> and Cl<sup>-</sup> ions from 15 to 4. With the ionic strength of the solution reduced, the formation of Cs<sup>+</sup>Cl<sup>-</sup> complexes was decreased. At these

lower ionic strengths, the Cs<sup>+</sup> ions did not tend to sorb to the aluminol surface, but instead bound adjacent to the center of the six-membered ring silica tetrahedral sheet in a transitory inner-sphere complex (Figure 9). The Cl<sup>-</sup> ions tend to form outer-sphere complexes that were attracted to the (001) aluminol plane.

In order to simulate a 0.01 M CsCl solution interacting with the (001) kaolinite surface, a two-layer slab model was constructed using a 24 x 12 x 2 supercell of the kaolinite unit cell. The interlayer distance was increased by 32 Å and populated with 15,030 H<sub>2</sub>O molecules. This large system (approximately 64,700 atoms) was then equilibrated using molecular dynamics and a constant-NVT ensemble for 20 psec with a time step of 0.001 psec. After reaching equilibrium, 4 Cs<sup>+</sup> and 4 Cl<sup>-</sup> ions (0.01 M CsCl) were inserted halfway along the interlayer distance and allowed to relax using an energy minimization scheme. A series of five NVT molecular dynamics runs were completed using a timestep of 0.001 psec and a simulation length of 250 psec. The equilibrium minimum energy configuration was again determined to be with the Cs<sup>+</sup> ions bound adjacent to the center of the six-membered ring silica tetrahedral sheet (Figure

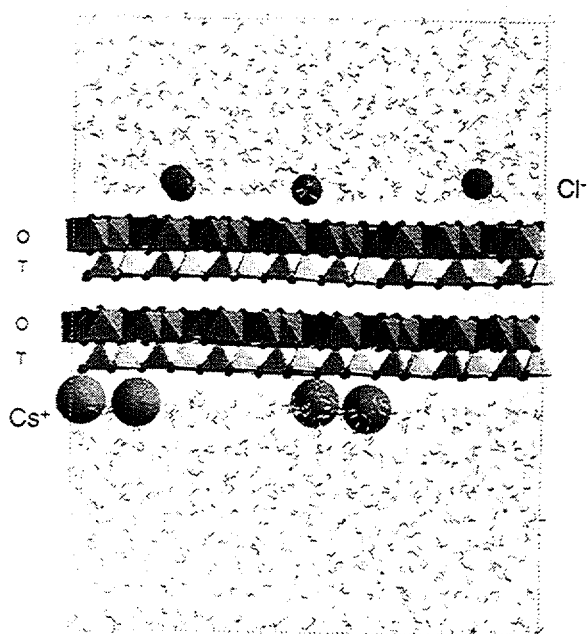


**Figure 8.** A graphical representation of a 0.5 M CsCl solution in steady-state equilibrium with a (001) kaolinite surface. At high ionic strengths, the formation of CsCl complexes occurs which can lead to  $\text{Cs}^+$  sorbing to the basal aluminol plane.

10). This inner-sphere complex can be transitory with the  $\text{Cs}^+$  ion desorbing from the surface and then either resorbing or going back into solution (Figure 11).

#### 4.4.2.2 Montmorillonite

Similar molecular dynamics simulations were completed for the montmorillonite basal surfaces interacting with either a  $\text{Cs}^+$  or  $\text{Sr}^{2+}$  solution. Only one TOT sheet of the clay was used to represent the substrate surfaces. Due to the charged nature of the montmorillonite layers, only the metal cations were incorporated into the solution. This ensured a neutral system where the negative charge of the tetrahedrally- and octahedrally-substituted montmorillonite, is balanced by the solvated metal cations. The large systems (approximately 65,000 atoms), were first equilibrated using molecular dynamics at constant-NVT ensemble for 20 psec with a time step of 0.001 psec. After reaching equilibrium, the metal cation solute was inserted halfway along the interlayer distance and allowed to relax using an energy minimization

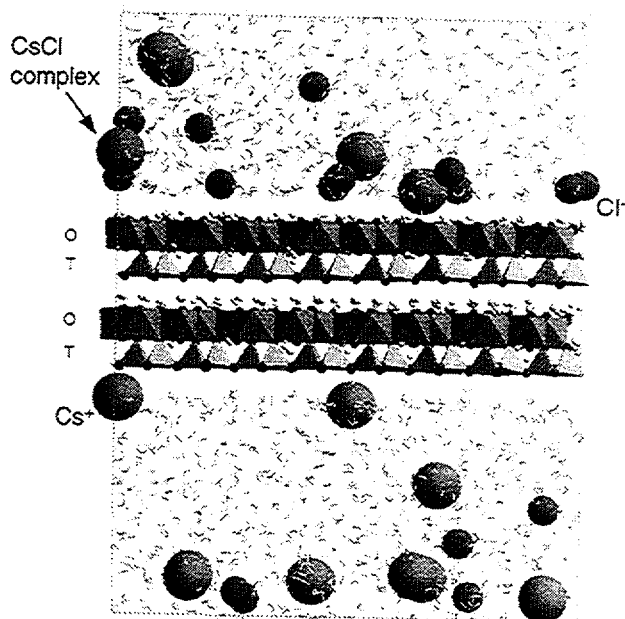


**Figure 9.** A graphical representation of a 0.1 M CsCl solution in steady-state equilibrium with a (001) kaolinite surface. This is the energetically-preferred configuration with the  $\text{Cs}^+$  ions sorbed to the basal tetrahedral plane and the  $\text{Cl}^-$  ions loosely sorbed to the basal aluminol plane.

scheme. A series of five NVT molecular dynamics runs were then completed, using a time-step of 0.001 psec and a simulation length of 250 psec.

Representative equilibrium results for the simulations of the  $\text{Cs}^+$  and  $\text{Sr}^{2+}$  systems interacting with montmorillonite are presented in Figures 12 and 13, respectively. The  $\text{Cs}^+$ -montmorillonite example exhibits a highly sorbing environment, with most of the  $\text{Cs}^+$  ions occurring as inner-sphere complexes and a few  $\text{Cs}^+$  ions remain solvated and isolated in the solution. The strongest sorption of the  $\text{Cs}^+$  occurs near montmorillonite sites associated with tetrahedral (Al for Si) and octahedral (Mg for Al) substitutions where there is an excess of negative charge. The transitory nature of the sorption, especially for outer-sphere  $\text{Cs}^+$  complexes, may lead to the clay substrate and perhaps later, resorption of the metal. This behavior underscores the need to apply statistically-sound methods for evaluating the sorption state of the system over the equilibrated simulation trajectory and for multiple simulations. The  $\text{Sr}^{2+}$ -montmorillonite example (Figure 13) indicates an equilibrated system in marked

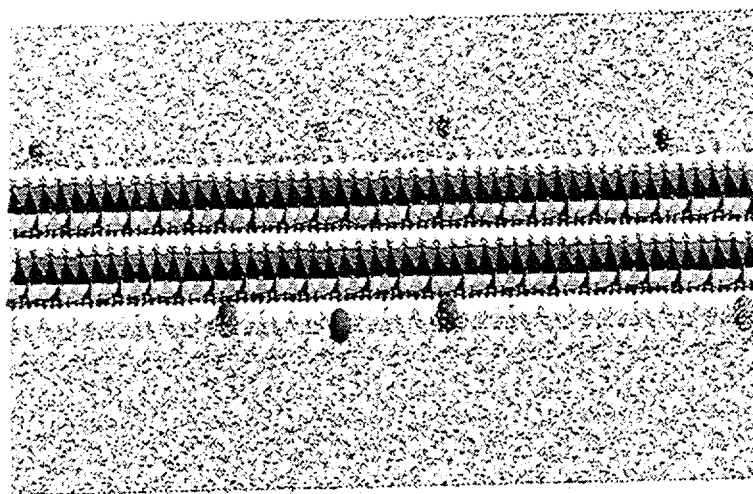


Figure 10. A graphical representation of a 0.01 M CsCl solution in steady-state equilibrium with a (001) kaolinite surface. This is the energetically-preferred configuration with the  $\text{Cs}^+$  ions sorbed to the basal tetrahedral plane and the  $\text{Cl}^-$  ions loosely sorbed to the basal aluminol plane.

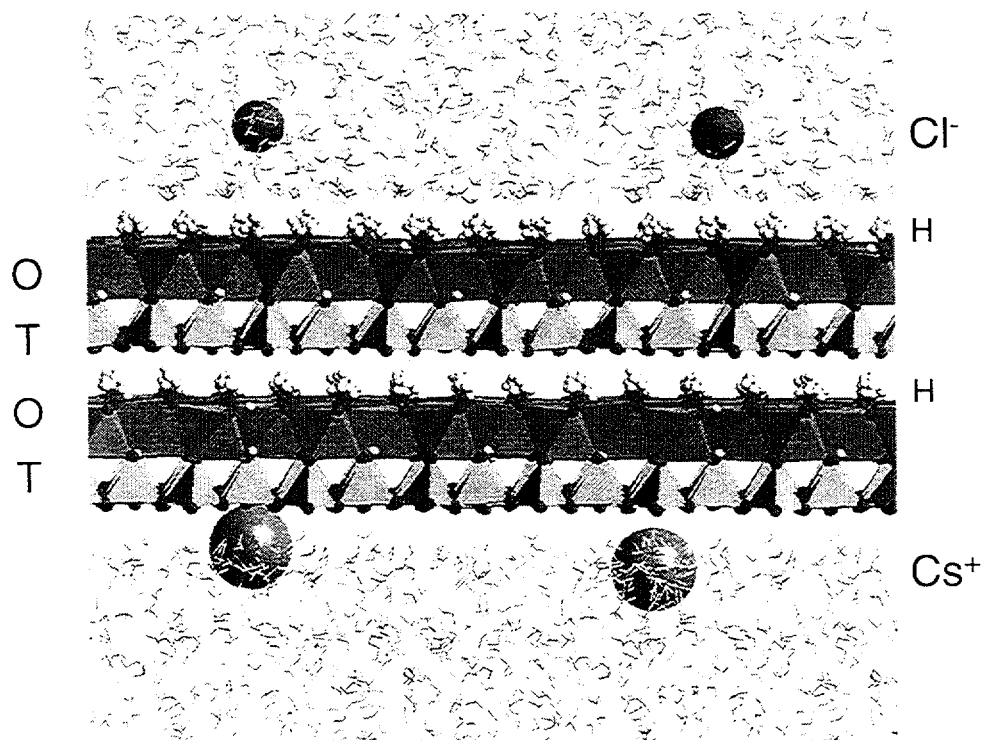
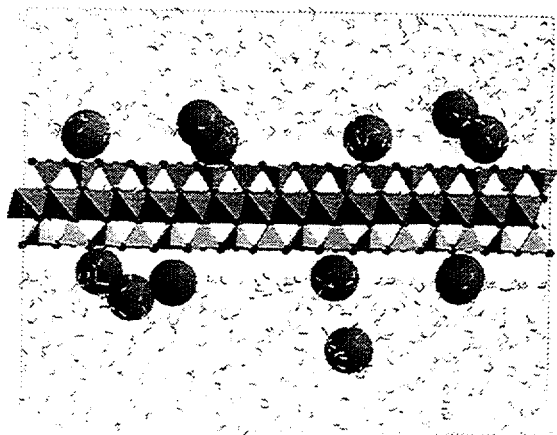
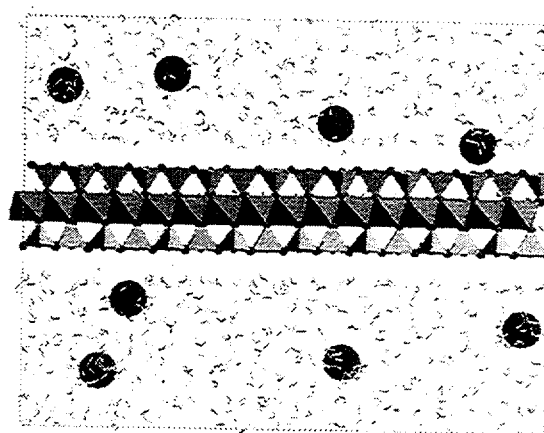


Figure 11. Details of the 0.01 M CsCl solution in steady-state equilibrium with a (001) kaolinite surface. Note that the  $\text{Cs}^+$  ions on the left are sorbed as an inner-sphere complex onto the basal aluminol plane while the one on the right is in the process of transitioning from an inner-sphere complex to a loosely sorbed outer-sphere complex. This second  $\text{Cs}^+$  is desorbed from the surface 10 psec after this dynamic configuration.



**Figure 12.** A graphical representation of a 0.1 M  $\text{Cs}^+$  solution in steady-state equilibrium with a (001) montmorillonite surface. This is the energetically preferred configuration with the  $\text{Cs}^+$  ions sorbed to the charged sites on the top and bottom tetrahedral planes.

contrast to those observed for the  $\text{Cs}^+$  simulations. The  $\text{Sr}^{2+}$  ion is rarely observed binding to the montmorillonite basal surface. When sorption does occur, it is often transitory and usually exists as an outer-sphere complex. All of the  $\text{Sr}^{2+}$ -montmorillonite simulations indicate a preference for the metal ion to be fully solvated by water molecules and remain in solution.



**Figure 13.** A graphical representation of a 0.1 M  $\text{Sr}^{2+}$  solution in steady-state equilibrium with a (001) montmorillonite surface. This is the energetically-preferred configuration with the  $\text{Sr}^{2+}$  ions sorbed to the charged sites on the top and bottom tetrahedral planes.

A set of molecular dynamics simulations was completed to examine the competition presented in Figure 14 where the  $\text{Cs}^+$  occurs fully sorbed to the basal surface, as mostly inner-sphere complexes and the  $\text{Sr}^{2+}$  remains in solution. Strontium ions often approach the basal surface during the simulation but never beyond a brief existence (up to 10 psec) as an outer-sphere complex. Statistical fluctuations in energy and ion trajectories will impact the evolution of these systems, especially when  $\text{Cs}^+$  remains at a sorption site preventing the near approach of a  $\text{Sr}^{2+}$  ion.

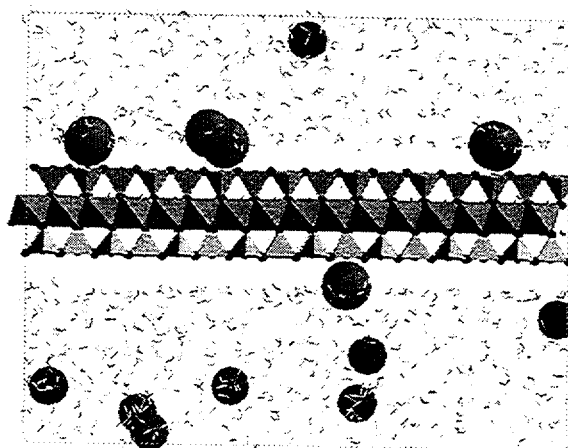


**Figure 14.** A graphical representation of 8  $\text{Cs}^+$  and 8  $\text{Sr}^{2+}$  ions in steady-state equilibrium with a (001) montmorillonite surface. This is the equilibrated configuration showing the competition between two different solvations, with the  $\text{Cs}^+$  ions are preferentially sorbed to the montmorillonite surface while the  $\text{Sr}^{2+}$  ions remain solvated.

## 5. CALCULATION OF DISTRIBUTION COEFFICIENTS

### 5.1 Kaolinite

The distribution coefficient ( $K_d$ ) is a measure of the ability of a material to sorb contaminants, and is defined as:

$$K_d = \left( \frac{C_i - C_f}{C_f} \right) \left( \frac{V_l}{M_s} \right) \quad (4)$$

where  $C_i$  is the initial concentration,  $C_f$  is the final concentration,  $V_l$  is the volume of the liquid in ml and  $M_s$  is the mass of the sorbent in grams. The higher the  $K_d$ , the greater the ability of a material to remove a contaminant from solution.

In order to evaluate the distribution coefficient of the kaolinite (001) surface to sorb  $\text{Cs}^+$  ions using the results of the computer simulations, the condition of sorption must first be defined. Based upon observing the sorption and desorption of  $\text{Cs}^+$  in the molecular dynamics simulations, we defined sorption as the  $\text{Cs}^+$  ion being within 5 Å of the plane of the aluminol groups or the oxygens on the silicate tetrahedral plane. Using this condition, the trajectory files for the molecular dynamics simulations were evaluated and the  $K_d$ 's were calculated. We determined a  $K_d$  of  $8 \pm 3$  ml/g for the 0.1 M CsCl solution and  $10 \pm 4$  ml/g for the 0.01 M CsCl solution. These results agree reasonably well with the experimental value of 12 ml/g (Brady *et al.*, 1998). It is important to note that the calculated  $K_d$  values assume that the entire contribution to  $\text{Cs}^+$  sorption can be attributed to the basal surfaces of the kaolinite and montmorillonite. In part this is a good assumption for smectite clays such as montmorillonite, but may be less valid for kaolinite where metal sorption onto edge sites can be significant (Brady *et al.*, 1996). Therefore,  $K_d$  values obtained from the kaolinite simulations should be considered as limiting cases, assuming the basal surfaces are the only sorbing surfaces. More detailed simulations incorporating the exposed edge sites—with their variable protonation state and therefore a function of pH—would be required to assess the relative role of edge *versus* basal sorption in kaolinite.

### 5.2 Montmorillonite

The significance of edge sites is less important for the  $K_d$  values derived from the montmorillonite simulations, where basal surfaces are the predominant sorp-

tion surface (Pabalan *et al.*, 1998). For the case of our montmorillonite simulations, we have determined a  $K_d$  of  $293 \pm 30$  ml/g to sorb  $\text{Cs}^+$  ions from a 0.1 M CsCl solution and a  $K_d$  of  $11 \pm 4$  ml/g to sorb  $\text{Sr}^{2+}$  ions from a 0.1 M  $\text{SrCl}_2$  solution.

The competitive sorption simulation of  $\text{Cs}^+$  and  $\text{Sr}^{2+}$  onto montmorillonite indicates the strong dominance of  $\text{Cs}^+$  over  $\text{Sr}^{2+}$  with  $K_d$  values that are in general agreement with the pure  $\text{Cs}^+$  solution.

### 5.3 Energetics and $K_d$ Values

A series of energy calculations was performed to examine the energy of various cations sorbed on kaolinite, montmorillonite and pyrophyllite, relative to the energies of the same cations being fully solvated by water molecules in solution. Pyrophyllite ( $\text{Si}_8\text{Al}_4\text{O}_{20}(\text{OH})_4$ ) represents a proxy for montmorillonite where there are no tetrahedral or octahedral substitutions; effectively this substrate represents weak montmorillonite sorption sites. The strong sorption sites on montmorillonite are basal sites associated with a tetrahedral substitution and nearby octahedral substitutions. Energy minimization calculations were performed for each configuration. Results are presented for  $\text{Cs}^+$ ,  $\text{Na}^+$ , and  $\text{Sr}^{2+}$  ions in Table 5. The reported energy values represent the optimum energy differences for the sorption site or hydration state.

The significance of these results is in comparing the energy values for each sorption site with the water hydration (solvation) energy for the chosen metal ion. For example,  $\text{Cs}^+$  indicates a fairly small solvation energy of -60 kcal/mol whereas the kaolinite and strong montmorillonite sorption energies are somewhat greater indicating a preference for  $\text{Cs}^+$  to be sorbed onto the clay. Similarly,  $\text{Na}^+$  exhibits a preference for only the strong montmorillonite site compared to remaining in solution. In contrast,  $\text{Sr}^{2+}$  shows an extremely large hydration energy of -315 kcal/mol that is related to the double ionic charge and relatively small ionic radius ( $\text{Na}^+ = 0.97$  Å;  $\text{Sr}^{2+} = 1.12$  Å;  $\text{Cs}^+ = 1.67$  Å). All of the clay substrates exhibit  $\text{Sr}^{2+}$  sorption energies that are similar to, or much less, than this large hydration energy. Therefore, it is not surprising to see limited sorption, if any at all, of  $\text{Sr}^{2+}$  in any of the previous molecular dynamics simulations.

**Table 5. Comparison of energy for various ions based on water solvation or clay surface sorption environment. The strong montmorillonite site corresponds to ion sorption near the tetrahedral aluminum and octahedral magnesium substitutions. The weak montmorillonite site represents a pyrophyllite-like smectite having no tetrahedral or octahedral substitutions.**

<b>Energy (kcal/mol)</b>	<b>Cs<sup>+</sup></b>	<b>Na<sup>+</sup></b>	<b>Sr<sup>2+</sup></b>
Water solvation	-60	-110	-315
Kaolinite	-74	-105	-275
Strong montmorillonite	-106	-142	-333
Weak montmorillonite	-37	-50	-163

## 6. CONCLUSIONS

Large-scale molecular dynamics were completed to model the sorption of  $\text{Cs}^+$  and  $\text{Sr}^{2+}$  ions onto the (001) planes of kaolinite and montmorillonite. Contrary to earlier simulations, (Cygan *et al.*, 1998), it was found that at high ionic strength cesium tends only to sorb to the aluminol plane through the formation of  $\text{CsCl}$  ion pairs. At lower concentrations, the  $\text{Cs}^+$  ions tend to sorb adjacent to the center of the six-membered ring silicate tetrahedral sheet in a transitory inner-sphere complex. Cesium sorption onto montmorillonite is

preferred over  $\text{Sr}^{2+}$  sorption due to the relatively large hydration energy of  $\text{Sr}^{2+}$  and relatively small sorption energy of  $\text{Sr}^{2+}$ . We are able to calculate distribution coefficients by defining the condition of sorption and by completing a series of large-scale and long-term molecular dynamics simulations in order to provide the necessary statistics. The results of this study indicate a strong link between the atomistic simulations and the macroscopic sorption properties.

## 7. SUGGESTIONS FOR FURTHER WORK

It is difficult to predict stable  $K_d$ 's for  $\text{Cs}^+$  sorbing to the (001) planes of kaolinite because of the formation of transitory inner- and outer-sphere complexes. Instead of trying to model the distribution coefficient, it seems worthwhile to evaluate the selectivity of a surface for the desired contaminant ion, and determine how that surface could be chemically or physically modified to enhance irreversible contaminant sorption.

The results of this study show that  $\text{Cs}^+$  preferentially binds to kaolinite and montmorillonite surfaces over  $\text{Sr}^{2+}$  because the  $\text{Cs}^+$  ion is poorly solvated by the water and migrates to the surface, while the  $\text{Sr}^{2+}$  is more strongly solvated by water and tends to remain in solution. We find that  $\text{Cs}^+$  and  $\text{Sr}^{2+}$  bind more effectively to montmorillonite than kaolinite due to the presence of negatively-charged sites due to  $\text{Al}^{+3}$  substituting for  $\text{Si}^{+4}$  and  $\text{Mg}^{+2}$  substituting for  $\text{Al}^{+3}$ . It is possible to examine the selectivity for a wide variety of cations to sorb to these and other layered materials. For the case of montmorillonite and kaolinite, our preliminary modeling studies suggest the following order of preference for major sorbing cations:  $\text{NH}_4^+ > \text{Cs}^+ > \text{K}^+ > \text{Na}^+ > \text{Li}^+$ . This interesting result suggests that  $\text{NH}_4^+$  will exchange for  $\text{Cs}^+$  on natural clays. This may be the mechanism that is responsible for the phenomenon known as "cask weeping", as atmospheric water contains significant amounts of dissolved  $\text{NH}_4^+$  ions. When a nuclear transport cask is covered with rain or dew, the  $\text{Cs}^+$  ions that are bound to natural clays stuck to the surface of the cask

desorb and are replaced by  $\text{NH}_4^+$  ions. A possible treatment to minimize this phenomenon would be to wash the cask with an ammonium solution prior to transport.

During the course of this study, we have developed more accurate forcefields for modeling the solvation of complex ions. We are now able to model the sorption of such radioactive ions as  $\text{I}^-$ ,  $\text{SeO}_4^{2-}$ ,  $\text{TcO}_4^-$ ,  $\text{Ra}^{2+}$ , uranium-carbonate complexes, as well as RCRA metals such as  $\text{CrO}_4^{2-}$  and  $\text{HAsO}_4^{2-}$ . Ultimately, our molecular simulation approach, when incorporating more efficient statistical mechanics algorithms such as thermodynamic integration, will allow the calculation of free energies for these complex systems.

Priorities for extensions of this study include the molecular dynamics simulation of more complex radionuclides such as the uranyl and uranyl-carbonate complexes. The latter are of significance due to their stability in solution at higher pH conditions leading to a reduction in the sorption of uranium. As noted above, the radioactive anions should be examined to derive relative rank ordering of sorption strengths. It would also be important to examine the influence of edge sites under various protonated states in order to assess the relative behavior of edge and basal sites for sorption. This last priority would be a difficult task due to the variation of acid pK values for the numerous cleavage surfaces and clay substitutions. However, a limited set of simulations may be helpful in providing a basis for analyzing sorption trends.

## 8. REFERENCES

- Adams, J.M. (1983) "Hydrogen atom positions in kaolinite by neutron profile refinement." *Clays and Clay Minerals*, 31, 352-356.
- Bish, D.L. (1993) "Rietveld refinement of the kaolinite structure at 1.5K". *Clays and Clay Minerals*, 41, 738-744.
- Bish, D.L. and Von Dreele, R.B. (1989) "Rietveld refinement of non-hydrous atomic positions in kaolinite." *Clays and Clay Minerals*, 37, 289-296.
- Brady, P.V., Cygan, R.T., and Nagy, K.L. (1996) "Molecular controls on kaolinite surface charge." *Journal of Colloid and Interface Science*, 183, 356-364.
- Brady, P.V., Cygan, R.T., and Nagy, K.L. (1998) "Surface charge and metal adsorption to kaolinite." In "Adsorption of Metals by Geomedia" (E.A. Jenne, Ed.), Academic Press, San Diego.
- Cygan, R.T., Nagy, K.L., and Brady, P.V. (1998) "Molecular models of cesium sorption on kaolinite." In "Adsorption of Metals by Geomedia" (E.A. Jenne, Ed.), Academic Press, San Diego.
- Cygan, R.T., Liang, J.J., Kalinichev, A.G. (2002) "Molecular models of hydroxide, oxyhydroxide, and clay phases, and the development of a general force-field." *Journal of Physical Chemistry*, in press.
- Delley, B. (2000) "From molecules to solids using the DMol3 approach." *Journal of Chemical Physics*, 113, 7756-7764.
- Gale, J.D. (1997) GULP: "A computer program for the symmetry adapted simulation of solids." *Philosophical Magazine B*, 73, 3-19.
- Giese, R.F. (1982) "Theoretical studies of the kaolin minerals: Electrostatic calculations." *Bulletin of Mineralogy*, 105, 417-424.
- Hess, A.C. and Saunders, V.R. (1992) "Periodic ab initio Hartree-Fock calculations of the low-symmetry mineral kaolinite." *Journal of Physical Chemistry*, 96, 4367-4374.
- Hobbs, J.D., Cygan, R.T., Nagy, K.L., Schultz, P.A., and Sears, M.P. (1997) "Ab initio energy minimization of the kaolinite crystal structure." *American Mineralogist*, 82, 657-662.
- Hohenberg, P. and Kohn, W. (1964) "Inhomogeneous electron gas." *Physical Review*, 136, 864-861.
- Kim, Y., Cygan, R.T., and Kirkpatrick, R.J. (1996a) "<sup>133</sup>Cs NMR and XPS investigation of cesium adsorbed onto clay minerals and related phases." *Geochimica et Cosmochimica Acta*, 60, 1041-1052.
- Kim, Y., Kirkpatrick, R.J., and Cygan, R.T. (1996b) "<sup>133</sup>Cs NMR study of cesium on the surfaces of kaolinite and illite." *Geochimica et Cosmochimica Acta*, 60, 4059-4074.
- Kim, Y. and Kirkpatrick, R.J. (1997) "<sup>23</sup>Na and <sup>133</sup>Cs NMR study of cation adsorption on mineral surfaces: local environments, dynamics, and effects of mixed cations." *Geochimica et Cosmochimica Acta*, 61, 5199-5208.
- Kim, Y., Kirkpatrick, R.J. (1998) "NMR T<sub>1</sub> relaxation study of <sup>133</sup>Cs and <sup>23</sup>Na adsorbed onto illite." *American Mineralogist*, 83, 661-665.
- Kohn, W., and Sham, L.J. (1965) "Self-consistent equations including exchange and correlation effects." *Physical Review A*, 140, 1133-1138.
- Komarneni, S. (1978) "Cesium sorption and desorption behavior of kaolinites." *Soil Science Society of America Journal*, 42, 531-532.
- Krumhansl, J.L., Brady, P.V., and Anderson, H.L. (2001) "Reactive barriers for <sup>137</sup>Cs retention." *Journal of Contaminant Hydrology*, 47, 233-240.
- Michaelian, K.H., Lapidés, I., Lahav, N., Yariv, S., and Brodsky, I. (1998a) "Infrared study of the intercalation of kaolinite by caesium bromide and caesium iodide." *Journal of Colloid and Interface Science*, 204, 389-393.
- Michaelian, K.H., Zhang, S.L., Yariv, S., and Lapidés, I. (1998b) "Low-frequency raman spectra of kaolinite alkali halide complexes." *Applied Clay Science*, 13, 233-243.
- Molecular Simulations Inc. (1999) "Cerius-2 4.0 User Guide, Forcefield-Based Simulations." Molecular Simulations Inc., San Diego.

- Monkhorst, H.J., and Pack, J.D. (1976) "Special points for Brillouin-zone integrations." *Physical Review B*, 13, 5188-5192.
- Nagy, K.L., Cygan, R.T., and Brady, P.V. (1995) "Kaolinite morphology: AFM observations, model predictions, and adsorption site density." *Clay and Minerals Society Program Abstracts*, 32, 95.
- Pabalan, R.T., Turner, D.R., Bertetti, P., and Prikryl, J. D. (1998) "Uranium<sup>VI</sup> sorption onto selected mineral surfaces." In *Adsorption of Metals by Geomedia* (E.A. Jenne, Ed.), Academic Press, San Diego.
- Neder, R.B., Burghammer, M., Grasl, T., Schulz, H., Bram, A., and Fiedler, S. (1999) "Refinement of the kaolinite structure from single-crystal synchrotron data." *Clays and Clay Minerals*, 47, 487-494.
- Ohtaki, H. and Radnai, T. (1993) "Structure and dynamics of hydrated ions." *Chemical Reviews*, 93, 1157-1204.
- Perdew, J.P. and Wang, Y. (1992) "Accurate and simple analytic expression of the electron-gas correlation energy." *Physical Review B*, 45, 13244-13249.
- Pickett, W.E. (1989) "Pseudopotential methods in condensed matter applications." *Computational Physics Reports*, 9, 115-197.
- Saiers, J.E. and Hornberger, G.M. (1999) "The influence of ionic strength on the facilitated transport of cesium by kaolinite colloids." *Water Resources Research*, 35, 1713-1727.
- Smith, D.E. and Dang, L.X. (1994a) "Computer simulations of NaCl association in polarizable water." *Journal of Chemical Physics*, 100, 3757-3766.
- Smith, D.E. and Dang, L.X. (1994b) "Computer simulations of cesium-water clusters: Do ion-water clusters form gas-phase clathrates?" *Journal of Chemical Physics*, 101, 7873-7881.
- Telemen, O., Jonsson, B., and Engstrom, S. (1987) "A molecular dynamics simulation of a water model with intramolecular degrees of freedom." *Molecular Physics*, 60, 193-203.
- Tsipursky, S.I. and Drits, V.A. (1984) "The distribution of octahedral cations in the 2:1 layers of dioctahedral smectites studied by electron diffraction." *Clay Minerals*, 19, 177-193.
- Vanderbilt, D. (1990) "Soft self-consistent pseudopotentials in a generalized eigenvalue formalism." *Physical Review B*, 41, 1990.
- Weiss, C.A., Jr., Kirkpatrick, R.J., Altaner, S.P. (1990) "The structural environments of cations adsorbed onto clays: <sup>133</sup>Cs variable-temperature MAS NMR spectroscopy study of hectorite." *Geochimica et Cosmochimica Acta*, 54, 1655-1669.
- Westrich, H.R., Cygan, R.T., Brady, P.V., Nagy K.L., Anderson, H.L., Kim, Y., and Kirkpatrick, R.J. (1995) "The sorption behavior of Cs and Cd onto oxide and clay surfaces." In *Proceeding of the Waste Management Conference, WM'95*, 24-4. *Folio Infobase*.
- Young, R.A. and Hewatt, A.W. (1988) "Verification of the triclinic crystal structure of kaolinite." *Clays and Clay Minerals*, 36, 225-232.

**BIBLIOGRAPHIC DATA SHEET**

(See instructions on the reverse)

1. REPORT NUMBER  
(Assigned by NRC, Add Vol., Supp., Rev.,  
and Addendum Numbers, if any.)

NUREG/CR-6757

2. TITLE AND SUBTITLE

Large-Scale Molecular Dynamics Simulations of Metal Sorption onto the Basal Surfaces of Clay Minerals

3. DATE REPORT PUBLISHED

MONTH YEAR

January 2002

4. FIN OR GRANT NUMBER

W6811

5. AUTHOR(S)

D.M. Teter and R.T. Cygan

6. TYPE OF REPORT

7. PERIOD COVERED (Inclusive Dates)

December 1999 to November 2001

8. PERFORMING ORGANIZATION - NAME AND ADDRESS (If NRC, provide Division, Office or Region, U.S. Nuclear Regulatory Commission, and mailing address; if contractor, provide name and mailing address.)

Geochemistry Section  
Sandia National Laboratories  
Albuquerque, NM 87185-0750

9. SPONSORING ORGANIZATION - NAME AND ADDRESS (If NRC, type "Same as above"; if contractor, provide NRC Division, Office or Region, U.S. Nuclear Regulatory Commission, and mailing address.)

Division of Systems Analysis and Regulatory Effectiveness  
Office of Nuclear Regulatory Research  
U.S. Nuclear Regulatory Commission  
Washington, DC 20555-0001

10. SUPPLEMENTARY NOTES

11. ABSTRACT (200 words or less)

Large-scale molecular dynamics computer simulations have been completed to evaluate the sorption of Cs<sup>+</sup>, Sr<sup>2+</sup>, and other related ions onto the (001) basal planes of kaolinite and montmorillonite. Simulations were undertaken as a function of metal ion concentration to evaluate sorption mechanisms and to determine distribution coefficients (K<sub>d</sub>'s). The simulations show that Cs<sup>+</sup> ions bind to both kaolinite and montmorillonite, while Sr<sup>2+</sup> ions tend to remain in solution. At high ionic strengths (greater than 0.5 M), the fundamental mechanism for Cs<sup>+</sup> sorption to the aluminol plane of kaolinite is through the formation of CsCl complexes where the Cl<sup>-</sup> ion is loosely bound to the outer hydroxyl groups. At lower concentrations (0.1 M and 0.01 M), the Cs<sup>+</sup> ions do not sorb to the aluminol plane, but prefer to bind adjacent to the center of the six-membered ring silica tetrahedral sheet as an inner-sphere complex. We have determined a K<sub>d</sub> of 10 ± 4 ml/g for kaolinite to sorb Cs<sup>+</sup> ions from a 0.01M CsCl solution, and a K<sub>d</sub> of 0 for kaolinite to sorb Sr<sup>2+</sup> ions from a 0.01M SrCl<sub>2</sub> solution. For the case of montmorillonite, we have determined a K<sub>d</sub> of 293 ± 30 ml/g to sorb Cs<sup>+</sup> ions from a 0.1M CsCl solution, and a K<sub>d</sub> of 11 ± 4 ml/g to sorb Sr<sup>2+</sup> ions from a 0.1M SrCl<sub>2</sub> solution. The montmorillonite sorbs the cations more effectively than kaolinite because it has negatively-charged sorption sites that are created by isomorphic substitutions on both tetrahedral and octahedral sites. Calculations show that the Sr<sup>2+</sup> ion is solvated more strongly than Cs<sup>+</sup> and is not sorbed by the kaolinite or montmorillonite surfaces. Directions for further work are outlined and prioritized.

12. KEY WORDS/DESCRIPTORS (List words or phrases that will assist researchers in locating the report.)

sorption, adsorption, desorption, Cs sorption, Sr sorption, sorption on clay, radionuclide transport

13. AVAILABILITY STATEMENT

unlimited

14. SECURITY CLASSIFICATION

(This Page)

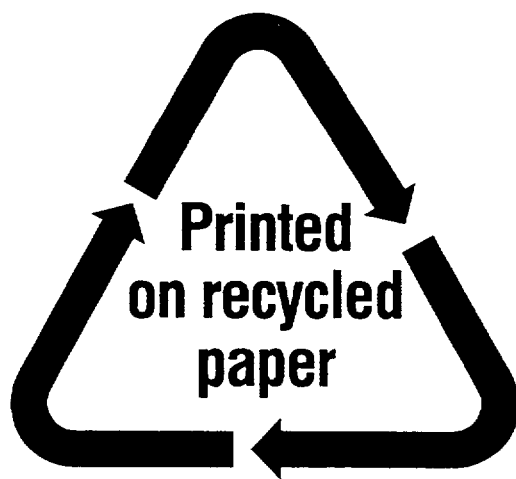
unclassified

(This Report)

unclassified

15. NUMBER OF PAGES

16. PRICE



Federal Recycling Program

**UNITED STATES  
NUCLEAR REGULATORY COMMISSION  
WASHINGTON, DC 20555-0001**

---

OFFICIAL BUSINESS  
PENALTY FOR PRIVATE USE, \$300